

Dual-pump manipulation of ultrafast demagnetization in TbFeCo

Tuyuan Cheng,^{1,2} Jing Wu,^{1,3,*} Tao Liu,⁴ Xiao Zou,¹ Jianwang Cai,⁴ Roy W. Chantrell,¹ and Yongbing Xu^{2,3}

¹*Department of Physics, University of York, Heslington, York YO10 5DD, United Kingdom*

²*Spintronics and Nanodevice Laboratory, Department of Electronics, University of York, Heslington, York YO10 5DD, United Kingdom*

³*York-Nanjing Joint Center (YNJC) for Spintronics and nano-engineering, Nanjing University, Nanjing 210093, China*

⁴*Institute of Physics, Chinese Academy of Sciences, Beijing 100190, China*

(Received 10 July 2015; revised manuscript received 14 January 2016; published 1 February 2016)

Laser-induced ultrafast demagnetization in TbFeCo has been studied with a dual-pumping system. Five different laser fluence combinations were applied at three different time intervals between two pump pulses. The experimental results are also compared with computational simulations using the atomistic model. Importantly, this demagnetization can be controllably manipulated in both its magnitude and temporal response.

DOI: [10.1103/PhysRevB.93.064401](https://doi.org/10.1103/PhysRevB.93.064401)

I. INTRODUCTION

Laser-induced ultrafast demagnetization has been investigated for many years [1–10] since Beaurepaire *et al.* first demonstrated it in ferromagnetic Ni film [1], and it is still one of the most important issues that could provide opportunities for a greater fundamental understanding of correlated phenomena in solid-state matter and magnetic recording techniques. A typical way to study the ultrafast dynamic process is to use a stroboscopic pump-probe system, with a high energy laser pulse acting as a pump to trigger the magnetization dynamics, and a low energy laser pulse acting as a probe, to detect the change in the reflectivity and magnetization dynamics via the magneto-optical Kerr effect (MOKE). The pump-probe scheme can monitor the electron temperature and magnetization simultaneously [2].

It has been shown that the reduction of the magnetization is increased with the increasing laser pump fluence [11,12]. In 2000, Zhang and Hübner [12] theoretically investigated the laser-induced ultrafast demagnetization using two 10 fs laser pulses as the pump source (P1 and P2). They found that one cannot only manipulate the drop in magnetization by choosing suitable pump intensities (varying the intensities of P1 and P2), but also tune its temporal sequence by setting different delays between these two pumps (increasing the delay between them from 0 to 50 fs and 80 fs).

Here we present a time-resolved investigation on the laser-induced ultrafast demagnetization of TbFeCo sample using pump-probe polar magneto-optical Kerr effect. The ultrafast demagnetization of the TbFeCo sample has been excited by two laser pump pulses in sequence with variable laser fluence and the time interval between them. The dual-pumping scheme was expected to provide an effective way to control the magnitude and temporal response of ultrafast demagnetization, which could be used as a future magnetic recording technique, to record information to magnetic materials within a desired (often short) time scale [12].

This paper is organized as follows: Experimental details including sample characteristics, optical setup, and low temperature system are described in Sec. II. Section III provides an introduction of the atomistic model used for theoretical

simulations in this project. In Secs. IV and V the results taken from both the single-pumping system and dual-pumping system are compared with computational simulations using the atomistic model. Finally, a conclusion is given in Sec. VI to indicate the importance of this dual-pumping manipulation technique.

II. EXPERIMENTAL DETAILS

TbFeCo, an amorphous RE-TM ferromagnetic alloy, was chosen for the project due to its large orbital moment and high magnetic anisotropy. The dots with a diameter of 300 μm and a thickness of 20 nm were grown on a glass substrate at ambient temperature by direct current magnetron sputtering using a metal mask. To deposit the TbFeCo onto the substrate, the Tb and Co was sputtered symmetrically onto an Fe target and the final composition was determined by inductively coupled plasma-atomic emission spectroscopy (ICP-AES). The base pressure of the sputtering system was less than 4×10^{-5} Pa and the Ar pressure was 0.5 Pa during sputtering. The TbFeCo film was covered by a 4 nm Ta layer to protect the sample against oxidation. Sputtering rates for TbFeCo and Ta are about 0.09 and 0.11 nm/s, respectively. A polar MOKE hysteresis loop measurement has been performed at room temperature, and this showed that the TbFeCo sample has a very strong perpendicular anisotropy with a coercivity of 1160 Oe and a saturation field of 2390 Oe, as shown in Fig. 1. A 4 kOe external magnetic field was applied perpendicular to the sample surface, which was big enough to ensure the sample was always at the same initial magnetic state before the pump pulses triggering the ultrafast demagnetization.

This experiment was performed at room temperature, we used a stroboscopic dual-pumping system to investigate the demagnetization in an ultrafast time scale. A femtosecond Ti:sapphire pulsed laser system, on loan from the Central Laser Facility, Rutherford Appleton Laboratory, with a pulse duration of 150 fs, a central wavelength of 800 nm, and a repetition rate of 1 kHz, was used as the laser source. An ultrafast beam sampler was used to split the laser beam into two parts. The transmitted beam (with about 90% of the total energy) was routed around an optical delay line, and then split optically into two pumps (Pump1 and Pump2) via a beam splitter; while the reflected beam (with about 10% of the total energy) acted as a probe, as schematically shown in Fig. 2.

*jing.wu@york.ac.uk

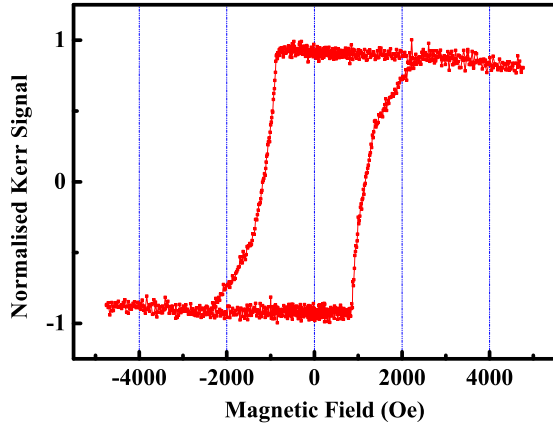


FIG. 1. Hysteresis loop of TbFeCo, measured at room temperature.

The time delay between Pump1 and probe was controlled by delay line 1, with 16.7 fs resolution over a 1 ns range, while the time delay between Pump1 and Pump2 was tuned by delay line 2 with a differential micrometer that has a corresponding resolution of 3.3 fs over 1.67 ps range.

The wavelength of the pulses in the pump path was maintained at 800 nm, while the wavelength of the pulses in the probe path was set to 400 nm by doubling the frequency using a BBO crystal. Both Pump1 and Pump2 were focused and overlapped on the sample to a spot diameter of around 500 μm , while the probe beam was linearly polarized, focused to a 50 μm spot and centered on the pump beam. There are different ways of getting the spot size, such as calculating by using the optical parameters, or measuring the FWHM (full-width at half-maximum) of a properly exposed image. In our experiment, a dotted sample (dot diameter: 300 μm) was used as a reference. The reflection was checked when manually scanning a pump across the sample dot, by which the focused

TABLE I. Summary of the various combinations of laser pump fluences and time intervals used in the dual-pump experiment.

Total fluence (Pump1 + Pump2) (J/m^2)	Pump1 (J/m^2)	Pump2 (J/m^2)	Time intervals between Pump1 and Pump2 (ps)
5.3	3.3	2	0.5, 1
	4.3	1	0.5, 1
4.8	3.3	1.5	0, 0.5, 1
	4.3	0.5	0.5, 1
4.3	3.3	1	0, 0.5, 1

beam spot size can be estimated. Also, when the pump intensity was increased to a certain level, that specific sample dot was completely burned. This was another evidence that the spot size of the pump was bigger than the dot, thus should be bigger than 300 μm . The laser pulse fluence is largely determined by its estimated spot size. The difference in calculating/measuring the spot size could be the main reason behind the relatively low pump fluence quoted here to other experiments [13,14]. The fluence ratio between the probe and pump was about 1/50. A CCD camera system was set to collect the scattered light from both pump and probe pulses, which was used to check the pump-probe overlapping, to make sure the pump beams and probe beam were overlapped at exactly the same position on the sample.

The fluence of Pump1 or Pump2 can be varied by using a separate attenuator. Both Pump1 and Pump2 approached the sample surface at an angle of 20 deg while the probe approached at near normal incidence. The reflected probe beam was directed into a bridge detector, where the difference (Kerr rotation) and sum (reflectivity) of the photodiodes were recorded. An optical chopper and a lock-in amplifier were used to detect the difference between pump on and off, and the Kerr rotation was averaged over 30 000 pulses on each different delay, both of which were effective ways to improve the signal-noise ratio. The combination of different time intervals and laser fluences between Pump1 and Pump2 are summarized in Table I.

III. ATOMISTIC MODEL

In Ref. [15] Mendil *et al.* investigated the role of femtosecond heated electrons by comparing ultrafast demagnetization with simulations. In our case, an atomistic model was chosen to reproduce the experimental results. The atomistic model used here was developed from the spin model described in Ref. [16], and is outlined briefly here. The system is viewed on an atomistic scale with each atom in the lattice represented by a magnetic moment. The basis of the model is the numerical solution of a set of coupled Landau-Lifshitz-Gilbert (LLG) equations of motion for the magnetic moments in an effective field. The effective field combines the Hamiltonian contribution and a thermal noise contribution. An extended Heisenberg spin Hamiltonian is used, comprised of exchange, uniaxial anisotropy, and Zeeman energies. The Hamiltonian is

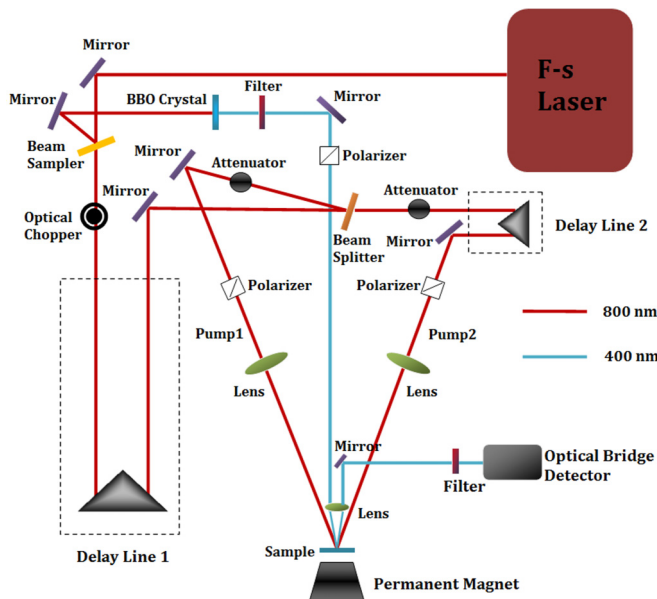


FIG. 2. Schematic diagram of the dual-pumping system.

given by

$$\mathcal{H} = - \sum_{i \neq j} J_{ij} \mathbf{S}_i \cdot \mathbf{S}_j - \sum_i d_z \mathbf{S}_{i,z}^2 - \sum_i \mu_i \mathbf{S}_i \cdot \mathbf{B}, \quad (1)$$

with $\mathbf{S} = \boldsymbol{\mu}/|\mu_s|$, where μ_s is the magnitude of the magnetic moment. Here J_{ij} is the exchange integral between spins i and j , limited here to nearest neighbors, d_z is the uniaxial anisotropy constant along the z axis, \mathbf{S}_i is the normalized spin at site i , and \mathbf{B} is the applied field in Tesla. We have used a simpler Hamiltonian than in Mryasov *et al.*'s in Ref. [16]. The reason is that the Hamiltonian in Ref. [16] is long ranged and computationally expensive, and here we are looking at the basic dynamics of the dual-pump process for which a simpler model suffices.

The magnetization dynamics is described by the Landau-Lifshitz-Gilbert equation for atomic spins written as

$$\frac{\partial \mathbf{S}_i}{\partial t} = - \frac{\gamma_0}{(1 + \lambda^2)} \mathbf{S}_i \times (\mathbf{H}_{\text{eff}} + \lambda \mathbf{S}_i \times \mathbf{H}_{\text{eff}}), \quad (2)$$

with λ the coupling constant to the heat bath and γ_0 the gyromagnetic ratio. To couple the thermal reservoir to the spin system, Langevin dynamics [17] is applied using a stochastic noise term. This converts the LLG equation into a stochastic differential equation which can be written as a standard Langevin equation with multiplicative noise. We couple the magnetic spins to the electron system, this is based on previous studies of fast relaxation in transition metals [10] which concluded that only a coupling of the spins to the conduction electrons was sufficient to cause subpicosecond demagnetization. The total field includes the thermal noise term ζ :

$$\mathbf{H}_{\text{eff}} = - \frac{\partial \mathcal{H}}{\partial \mathbf{S}} + \zeta. \quad (3)$$

The stochastic process is assumed to be white noise with the following mean and variance:

$$\langle \zeta(t) \rangle = 0, \quad (4)$$

$$\langle \zeta_i(t) \zeta_j(t') \rangle = \delta_{ij} \delta(t - t') \frac{2\mu k_B T_e}{\gamma_0}, \quad (5)$$

with T_e the electron temperature. To model the heat bath to which the spin system is coupled we have employed the so-called two-temperature model [18]. The two-temperature model describes the change in the temperature of the electron and phonon baths under the action of a laser pulse, which is coupled directly to the electron bath which then transfers energy into the phonon and spin systems. The temperature dynamics are governed by two coupled differential equations:

$$C_e \frac{dT_e}{dt} = -G_{el}(T_l - T_e) + P(t), \quad (6)$$

$$C_l \frac{dT_l}{dt} = -G_{el}(T_e - T_l), \quad (7)$$

where C_e and C_l are the electron and phonon (lattice) heat capacities, T_l describes the phonon (lattice) temperature, $P(t)$ represents the input laser power, and G_{el} is the electron-phonon coupling factor. In the simulations G_{el} and C_l are taken to be independent of temperature which for the room

temperature calculations is a reasonable assumption. The parameters used were $G_{el} = 2 \times 10^{18} \text{ J m}^{-3} \text{ K}^{-1} \text{ s}^{-1}$, $C_l = 3 \times 10^6 \text{ J m}^{-3} \text{ K}^{-1}$, and $C_e(T_e) = 7 \times 10^2 T_e \text{ J m}^{-3} \text{ K}^{-1}$. The exchange integral $J_{ij} = 5.4 \times 10^{-21} \text{ J}$ per atomic link, anisotropy constant $K(T=0) = 9.3 \times 10^5 \text{ J m}^{-3}$. All these values are fitted to the experimental data. One also needs to initialize the following parameters when using the code for simulations: the duration of the pump pulse, the fluence of Pump1 and Pump2, and the time interval between these two pumps.

IV. SINGLE-PUMP MANIPULATION OF ULTRAFAST DEMAGNETIZATION

A series of time-resolved ultrafast demagnetizations induced by a single laser pump have been conducted at room temperature using different pump fluences before commencing the dual-pump manipulation measurements. The dynamic profiles of the ultrafast demagnetization and corresponding reflectivity curves at different pump fluences are shown in Fig. 3. The fluence range of the pump pulses was chosen from 2 to 6.1 J/m^2 .

The reflectivity profile obtained is a superposition of the electron temperature dynamics and the lattice temperature dynamics. As shown in Fig. 3(a), the reflectivity has a transient increase in its magnitude, and reaches a sharp peak at 500 fs after the pump excitation, which corresponds to the large rise in electron temperature caused by the arrival of the 150 fs laser pulse. The electron system then establishes thermal equilibrium with the lattice, creating the broader oscillations. In this experiment, the reflectivity curve seems to be dominated by the lattice temperature, since the electron temperature peak shown in the reflectivity data is not high in magnitude compared with that at electron-phonon (lattice) equilibrium. The oscillations in the reflectivity could be explained by the phonon mode excited by the pump pulses, in other words on the assumption that phonons are moving vertically in the form of stress waves and reflect off the interface with the glass substrate. The phonon mode is relatively weak when

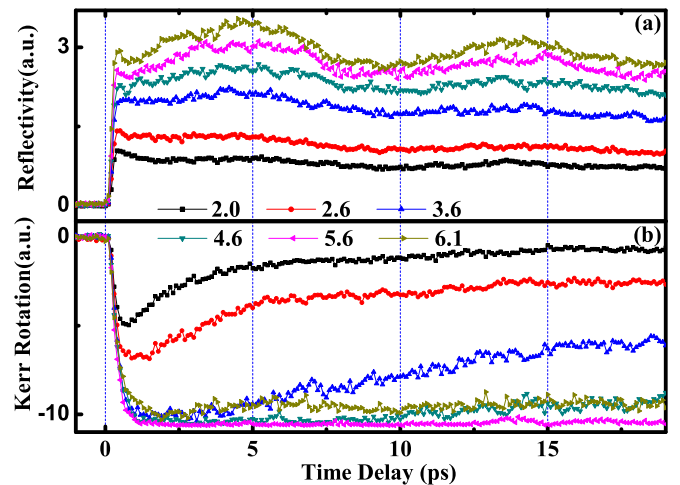


FIG. 3. Reflectivity (a) and demagnetization (b) curves induced by a single pumping system with increasing pump fluence (from 2 to 6.1 J/m^2).

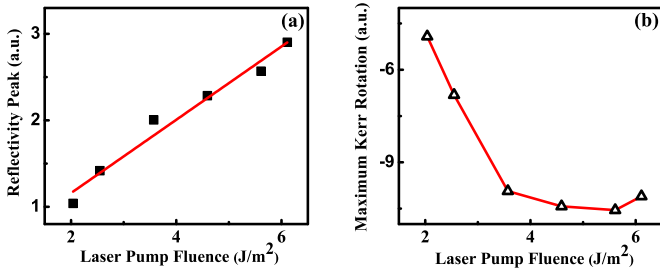


FIG. 4. (a) Reflectivity peak as a function of the increasing pump fluence (the red line is linear fit to the data points). (b) Kerr rotation peak as a function of the increasing pump fluence (the red line is a spline line as a guide to the eye).

the pump fluence is 2 and $2.6 J/m^2$, but becomes more obvious when the pump fluence was above $3.6 J/m^2$. The peak amplitudes of the reflectivity data are plotted as a function of the pump laser fluences in Fig. 4(a). It is shown that the electron temperature peak (represented by the peak in reflectivity) is linearly proportional to the increasing pump fluence, and the highest electron temperature is reached when the pump fluence is $6.1 J/m^2$.

Figure 3(b) shows a single pump manipulation of the ultrafast demagnetization while varying the pump fluence. The demagnetization lags the change in reflectivity by about 70 fs. The maximum reduction in demagnetization is achieved in less than 1 ps after excitation. The peak Kerr signals (Kerr rotation peak) are plotted as a function of the increasing pump fluence in Fig. 4(b). The maximum magnitude of the demagnetization (Kerr rotation peak) is shown to be proportional to the pump fluence but approaching a limit asymptotically. At this limit, complete demagnetization is achieved and no net magnetization remains. In this experiment, the sample is seen to be approaching the fully demagnetized state when the pump fluence is above $4.6 J/m^2$. $5.6 J/m^2$ is the largest pump fluence that can be safely performed on the sample, as the decreased demagnetization signal observed at $6.1 J/m^2$ indicates that sample has already been partially damaged by the laser pump. To avoid potential damage to the sample by intense laser pump pulses, the highest total fluence chosen in the dual-pumping studies was $5.3 J/m^2$, slightly less than the maximum fluence that has been safely used in the single-pumping system.

It is also interesting to note that the recovery rate of magnetization from the initial ultrafast demagnetization is inversely related to the laser pump fluence, which is consistent with Kazantseva *et al.*'s calculations in Ref. [10] and what Bunce *et al.* have found in Ref. [19]. This finding indicates that the recovery of magnetization is crucially dependent on the magnetic state achieved after pump laser excitation. The more the sample has been demagnetized, the slower the recovery rate would be. After complete demagnetization, the magnetization recovers by nucleation in random directions at scattered sites. This leads to considerable frustration and to the slow recovery. The magnetization recovery process is also thought to be influenced by the spin-lattice relaxation time, which is strongly related to the magnetocrystalline anisotropy energy [20]. With increasing laser fluence, higher electron and lattice temperatures can be achieved, in which

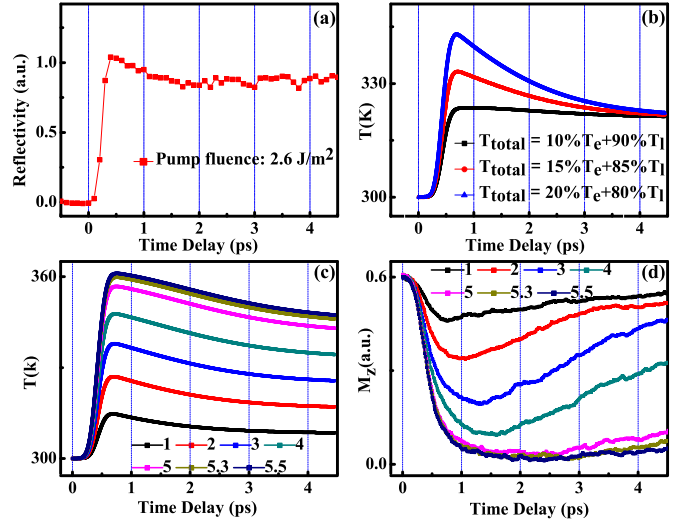


FIG. 5. (a) The reflectivity profile under a pump fluence of $2.6 J/m^2$ compared to (b) two-temperature model simulations with the same pump fluence but different mixing factor α . (c) Reflectivities produced by computational simulations with the mixing factor α as 0.15 (15%). (d) Demagnetizations produced by computational simulations with the mixing factor α as 0.15 (15%).

case the magnetocrystalline anisotropy as well as the spin-orbit coupling become weaker than before, thus leading to a relatively longer spin-lattice relaxation time and recovery process.

For the theoretical simulations based on the atomistic model, a group of simulations (modeling both reflectivity and demagnetization) with different pump fluences were performed. The pulse shape as a Gaussian function with 150 fs pulse width was chosen for the simulation. During the ultrafast demagnetization process, the electron temperature T_e increases rapidly after laser pulse excitation and usually reaches its peak temperature in less than 1 ps. It then reduces on the picosecond time scale to reach equilibrium with the phonon (lattice) temperature T_l . In this experiment, the reflectivity profile measured is a superposition of both T_e and T_l , in which case a mixing factor α was introduced for the calculation of the reflectivity in the simulations, to tune the contribution of T_e and T_l by using the following equation:

$$T_{total} = \alpha T_e + (1 - \alpha) T_l. \quad (8)$$

A range of α have been tested, and 0.15 (15%) was found to be the most suitable one to reproduce the reflectivity profile in the dual-pump simulations. Figures 5(a) and 5(b) compared the reflectivity profile under a pump fluence of $2.6 J/m^2$ with the two temperature model simulations. Clearly the simulation with α as 0.15 (15%) produced the best match to the experimental result.

As shown in Figs. 5(c) and 5(d), for single pump pulses, both the reflectivity and demagnetization simulation results have qualitatively reproduced the experimental data. It is shown that the system is approaching the fully demagnetized state when the total fluence is above $5 J/m^2$, further justifying the choice of $5.3 J/m^2$ as the maximum total fluence for (Pump1 + Pump2) in the dual-pump simulations.

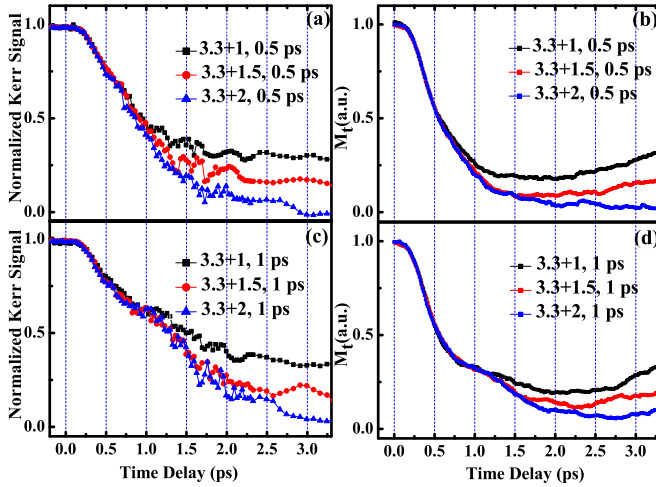


FIG. 6. (a) Fixed Pump1 (3.3 J/m^2) and variable Pump2 (1, 1.5, and 2 J/m^2) at a time interval of 0.5 ps (experiment). (b) Fixed Pump1 (3.3 J/m^2) and variable Pump2 (1, 1.5, and 2 J/m^2) at a time interval of 0.5 ps (simulation). (c) Fixed Pump1 (3.3 J/m^2) and variable Pump2 (1, 1.5, and 2 J/m^2) at a time interval of 1 ps (experiment). (d) Fixed Pump1 (3.3 J/m^2) and variable Pump2 (1, 1.5, and 2 J/m^2) at a time interval of 1 ps (simulation).

V. DUAL-PUMP MANIPULATION OF ULTRAFAST DEMAGNETIZATION

The chosen time intervals between Pump1 and Pump2 in the dual-pump manipulation experiment have been previously summarized in Table I. As demonstrated in Figs. 3(a) and 3(b), the electron temperature reached its peak value 500 fs (0.5 ps) after laser excitation while the maximum reduction of magnetization was achieved in just under 1 ps. The time interval 0.5 ps was chosen because Pump2 would be applied to the sample before the elevated electron temperature dropped down, and the time interval 1 ps was chosen as the maximum demagnetized state was just reached without any recovery yet.

Then we are in a position to investigate how the spin system can be manipulated by dual-pump excitation. First, Pump1 was set at a fixed fluence of 3.3 J/m^2 , with Pump2 increasing from 1 to 2 J/m^2 . The demagnetization curves taken at a time interval of 0.5 ps are shown in Fig. 6(a), while the ones taken at a time interval of 1 ps are shown in Fig. 6(c). It is shown that a pronounced additional reduction taking place when the second pump pulse arrived and triggered the further demagnetization. In Fig. 6(a), Pump2 arrives 0.5 ps after Pump1, the magnitude of the second reduction is increased with the increasing fluence of Pump2. In Fig. 6(c), Pump2 arrives 1 ps after Pump1, a similar demagnetization profile is observed, but the time interval between two pumps is more obvious this time, with a clear step between the first reduction and the second reduction. In both cases, the total reduction of magnetization was found to be proportional to the fluence of Pump2.

As pointed out by Zhang *et al.* in Ref. [12], one could have a very weak second reduction in magnetization if the first reduction has already driven the sample to a nearly complete demagnetized state (in which case the second reduction induced by Pump2 may not have an obvious impact on the change of magnetization because the demagnetization

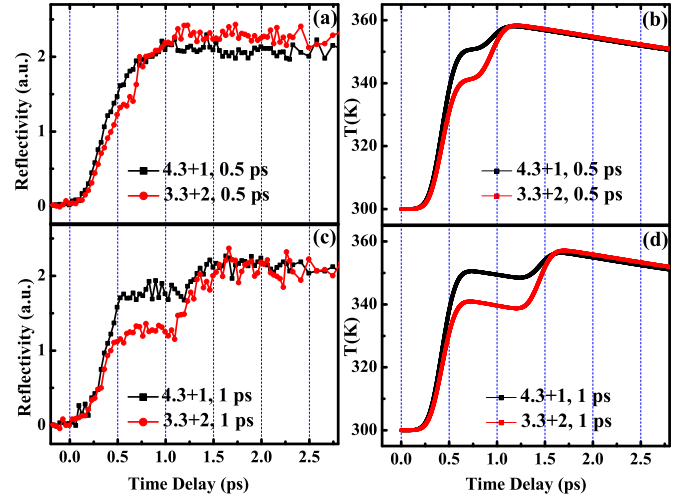


FIG. 7. (a) Reflectivity curves induced by dual-pump ($4.3 + 1 \text{ J/m}^2$ and $3.3 + 2 \text{ J/m}^2$) at a time interval of 0.5 ps (experiment). (b) Reflectivity curves induced by dual-pump ($4.3 + 1 \text{ J/m}^2$ and $3.3 + 2 \text{ J/m}^2$) at a time interval of 0.5 ps (simulation). (c) Reflectivity curves induced by dual-pump ($4.3 + 1 \text{ J/m}^2$) and ($3.3 + 2 \text{ J/m}^2$) at a time interval of 1 ps (experiment). (d) Reflectivity curves induced by dual-pump ($4.3 + 1 \text{ J/m}^2$) and ($3.3 + 2 \text{ J/m}^2$) at a time interval of 1 ps (simulation).

is almost saturated), and weakening the intensity of Pump1 (so the first reduction would only partially demagnetize the sample, giving Pump2 more freedom to manipulate the second reduction) is a possible way to enhance the additional reduction. The fluence of Pump1 chosen in this experiment was far away from the fluence that could fully demagnetize the sample, which gave the spin system more freedom to be manipulated by the second pump pulse. For the simulations, Pump1 was given a fixed fluence of 3.3 J/m^2 , while Pump2 was set at different fluences: 1, 1.5, and 2 J/m^2 . The computational simulations based on the atomistic model are compared with the experimental results, with a time interval of 0.5 ps shown in Fig. 6(b) and a time interval of 1 ps shown in Fig. 6(d). The simulations fit the experimental results quite well, which indicates the feasibility of using a second laser pump pulse to controllably manipulate the magnitude and response time in the ultrafast demagnetization process.

The experimental reflectivity and demagnetization results at a total pump fluence of 5.3 J/m^2 are compared with the computational simulations, in Figs. 7 and 8, respectively. As previously mentioned in Sec. IV, a mixing factor of 0.15 was chosen to tune the ratio between the electron temperature and the lattice temperature. This means the simulated reflectivity is by 15% electron temperature +85% lattice temperature. This also confirms that for our sample, the reflectivity is more sensitive to lattice temperature than electron temperature.

For Figs. 7(a) and 8(a), with a time interval 0.5 ps, further increase in reflectivity and further reduction in magnetization are small when Pump2 is 1 J/m^2 , but are increased when the fluence of Pump2 is increased to 2 J/m^2 . For Figs. 7(c) and 8(c), with a time interval 1 ps, the further increase in reflectivity and further reduction in magnetization become obvious at both 1 and 2 J/m^2 . The experimental and simulation results share

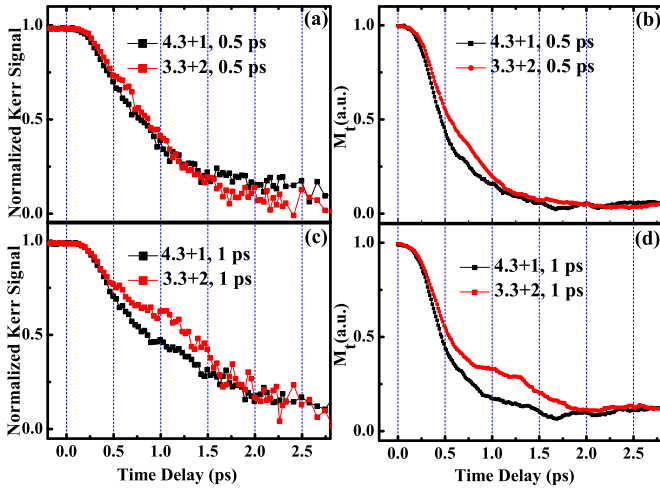


FIG. 8. (a) Demagnetization induced by dual-pump ($4.3 + 1$ J/m^2) and ($3.3 + 2$ J/m^2) at a time interval of 0.5 ps (experiment). (b) Demagnetization induced by dual-pump ($4.3 + 1$ J/m^2) and ($3.3 + 2$ J/m^2) at a time interval of 0.5 ps (simulation). (c) Demagnetization induced by dual-pump ($4.3 + 1$ J/m^2) and ($3.3 + 2$ J/m^2) at a time interval of 1 ps (experiment). (d) Demagnetization induced by dual-pump ($4.3 + 1$ J/m^2) and ($3.3 + 2$ J/m^2) at a time interval of 1 ps (simulation).

a very similar profile. It is interesting to note that for the same total pump fluence (5.3 J/m^2) but different combination and time interval between the two pump pulses, the peak temperature and total rate of demagnetization did not show a strong dependence on either the fluence combination or the time interval.

In Ref. [21], Figini *et al.* investigated the influence of the pulse length on the magnetization dynamics, and found the demagnetization observed in Ni caused by a picosecond laser pulse can be reconstructed from the response to a femtosecond pulse. They also demonstrated that the demagnetization after 10 ps only depends on total energy of the pulse, which is in line with our findings here. The results shown in Figs. 7 and 8 prove that in the dual-pumping system, the total magnitude of the demagnetization is determined by the total pump fluence, when the time interval between Pump1 and Pump2 is 0.5 and 1 ps. However, one can easily tune the magnitudes of the first reduction and the second reduction by changing the fluence ratio (Pump1/total or Pump2/total). Due to the limited loan period of the femtosecond laser system, no other measurements have been performed for the total pump fluence of 5.3 J/m^2 , but the simulation code based on the atomistic model provides us the opportunity to try some other combinations. In total, four different combinations were chosen ($4.3 + 1$, $3.3 + 2$, $2.3 + 3$, and $1.3 + 4$ J/m^2 , including the two that have previously been presented in Figs. 7 and 8). The time interval between Pump1 and Pump2 was varied from 0.5 to 1 ps. The simulation results of both reflectivities and demagnetizations are presented in Fig. 9, which again prove that the peak temperature and total demagnetization achieved are independent of the combinations.

Moreover, it is not just the magnitude of demagnetization that can be manipulated by choosing suitable dual-pump fluences, but also the temporal sequence can be easily tuned by

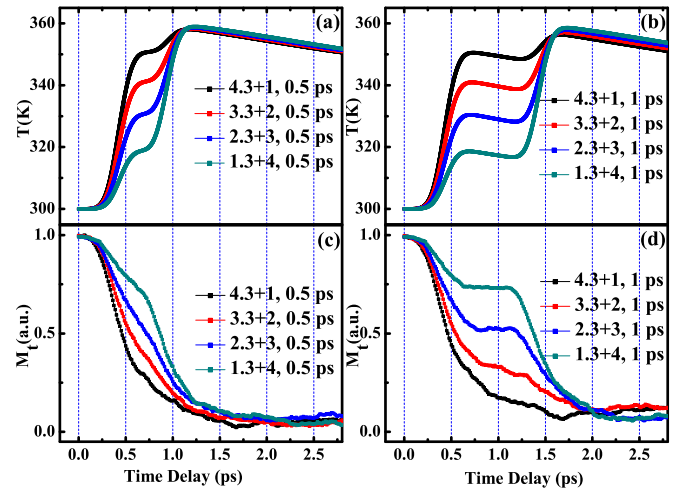


FIG. 9. Computational simulations with different dual-pump combinations and time intervals. (a) Reflectivity curves induced by dual-pump ($4.3 + 1$, $3.3 + 2$, $2.3 + 3$, and $1.3 + 4$ J/m^2) at a time interval of 0.5 ps. (b) Reflectivity curves induced by dual-pump ($4.3 + 1$, $3.3 + 2$, $2.3 + 3$, and $1.3 + 4$ J/m^2) at a time interval of 1 ps. (c) Demagnetization induced by dual-pump ($4.3 + 1$, $3.3 + 2$, $2.3 + 3$, and $1.3 + 4$ J/m^2) at a time interval of 0.5 ps. (d) Demagnetization induced by dual-pump ($4.3 + 1$, $3.3 + 2$, $2.3 + 3$, and $1.3 + 4$ J/m^2) at a time interval of 1 ps.

setting different time intervals. As shown in Fig. 10, dual-pump induced demagnetization with pump fluence of ($3.3 + 1$ J/m^2) and ($3.3 + 1.5$ J/m^2) have been compared with computational simulations with corresponding pump combinations, at three different time intervals. In both experimental and simulation results, it is clear that the additional reduction of magnetization

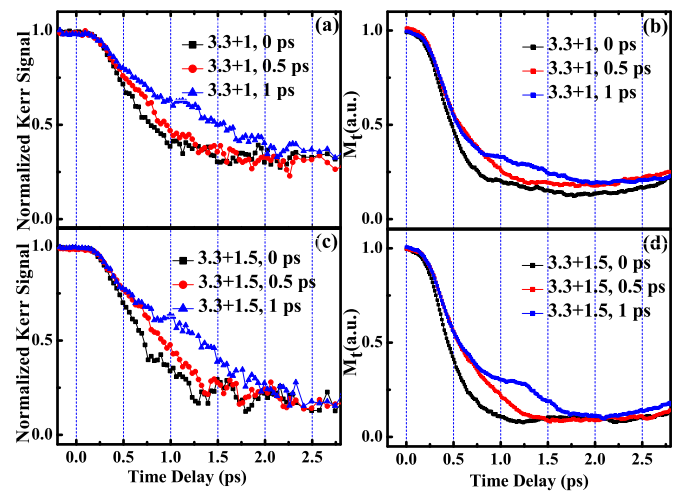


FIG. 10. (a) Demagnetization induced by dual-pumping system ($3.3 + 1$ J/m^2) at different time intervals (0 , 0.5 , and 1 ps) (experiment). (b) Demagnetization induced by dual-pumping system ($3.3 + 1$ J/m^2) at different time intervals (0 , 0.5 , and 1 ps) (simulation). (c) Demagnetization induced by dual-pumping system ($3.3 + 1.5$ J/m^2) at different time intervals (0 , 0.5 , and 1 ps) (experiment). (d) Demagnetization induced by dual-pumping system ($3.3 + 1.5$ J/m^2) at different time intervals (0 , 0.5 , and 1 ps) (simulation).

caused by the second pump pulse was moved from time 0 towards 0.5 ps and then 1 ps.

VI. CONCLUSION

A group of dual-pump induced ultrafast demagnetization measurements on TbFeCo sample have been presented and compared with computational simulations based on the atomistic model. Five different laser fluence combinations were applied at three different time intervals between two pump pulses. The additional reduction in magnetization excited by the second pump pulse demonstrates a controllable manipulation of the magnitude and temporal response of demagnetization dynamics, by tuning the fluence and time interval of the second pump. It is also proved by the two temperature model calculations that, with the same total pump fluence, the peak temperature and total demagnetization achieved are independent of the fluence combination between these two pumps. Moreover, the temporal response of the ultrafast demagnetization can be manipulated by setting different time intervals between Pump1 and Pump2 from 0 to 1 ps.

With the current perpendicular magnetic-recording era coming to an end, heat-assisted magnetic recording is expected to be the next decade technology to push the recording density to the next level. The findings here provide solid

experimental and theoretical evidence that the heating of the magnetization could be controlled by varying the fluence and time delay between two successive laser pump pulses. The spin system temperature, which was controlled by the fluence and temporal delay between the two pump pulses, was shown playing a key role for the demagnetization within the first couple of picoseconds. The fine tuning of the delay time between two pump pulses provides the flexibility of manipulating the temporal profile of the spin temperature. The findings here demonstrate that dual pumping is a controllable manipulation of both the magnitude and temporal response of the demagnetization dynamics, which would suggest a possible way to inscribe information to magnetic materials at a desired time scale and realize ultrafast temporal writing.

ACKNOWLEDGMENTS

The authors would like to thank the Central Laser Facility at the Rutherford Appleton Laboratory for the loan of the ultrafast femtosecond laser system. This work is also partially supported by the China Academy of Engineering Physics (Grant No. 2014CB921101), the National Natural Science Foundation of China (Grants No. 61274102, No. 61427812, and No. 11304148).

-
- [1] E. Beaurepaire, J. C. Merle, A. Daunois, and J. Y. Bigot, *Phys. Rev. Lett.* **76**, 4250 (1996).
 - [2] J. Hohlfeld, E. Matthias, R. Knorren, and K. H. Bennemann, *Phys. Rev. Lett.* **78**, 4861 (1997).
 - [3] A. Scholl, L. Baumgarten, R. Jacquemin, and W. Eberhardt, *Phys. Rev. Lett.* **79**, 5146 (1997).
 - [4] B. Koopmans, M. van Kampen, J. T. Kohlhepp, and W. J. M. de Jonge, *Phys. Rev. Lett.* **85**, 844 (2000).
 - [5] H. Regensburger, R. Vollmer, and J. Kirschner, *Phys. Rev. B* **61**, 14716 (2000).
 - [6] L. Guidoni, E. Beaurepaire, and J.-Y. Bigot, *Phys. Rev. Lett.* **89**, 017401 (2002).
 - [7] E. Beaurepaire, G. M. Turner, S. M. Harrel, M. C. Beard, J. Y. Bigot, and C. A. Schmuttenmaer, *Appl. Phys. Lett.* **84**, 3465 (2004).
 - [8] M. Vomir, L. H. F. Andrade, L. Guidoni, E. Beaurepaire, and J. Y. Bigot, *Phys. Rev. Lett.* **94**, 237601 (2005).
 - [9] T. Y. Cheng, L. Atkinson, J. Wu, R. W. Chantrell, J. Sizeland, Y. M. Lu, J. W. Cai, and Y. B. Xu, *IEEE Trans. Magn.* **50**, 6101004 (2014).
 - [10] N. Kazantseva, U. Nowak, R. W. Chantrell, J. Hohlfeld, and A. Rebei, *Europhys. Lett.* **81**, 27004 (2008).
 - [11] X. Liu, Z. Xu, R. Gao, H. Hu, Z. Chen, Z. Wang, J. Du, S. Zhou, and T. Lai, *Appl. Phys. Lett.* **92**, 232501 (2008).
 - [12] G. P. Zhang and W. Hübner, *Phys. Rev. Lett.* **85**, 3025 (2000).
 - [13] B. Vodungbo, J. Gautier, G. Lambert, A. B. Sardinha, M. Lozano, S. Sebban, M. Ducouso, W. Boutu, K. Li, B. Tudu, M. Tortarolo, R. Hawaldar, R. Delaunay, Vi. López-Flores, J. Arabski, C. Boeglin, H. Merdji, P. Zeitoun, and J. Lüning, *Nat. Commun.* **3**, 999 (2012).
 - [14] I. Radu, K. Vahaplar, C. Stamm, T. Kachel, N. Pontius, H. A. Dušrr, T. A. Ostler, J. Barker, R. F. L. Evans, R. W. Chantrell, A. Tsukamoto, A. Itoh, A. Kirilyuk, Th. Rasing, and A. V. Kimel, *Nature (London)* **472**, 205 (2011).
 - [15] J. Mendil, P. Nieves, O. Chubykalo-Fesenko, J. Walowski, T. Santos, S. Pisana, and M. Munzenberg, *Sci. Rep.* **4**, 3980 (2014).
 - [16] O. N. Mryasov, U. Nowak, K. Y. Guslienko, and R. W. Chantrell, *Europhys. Lett.* **69**, 805 (2005).
 - [17] A. Lyberatos, D. V. Berkov, and R. W. Chantrell, *J. Phys.: Condens. Matter* **5**, 8911 (1993).
 - [18] J. Chen, D. Tzou, and J. Beraun, *Int. J. Heat Mass Transfer* **49**, 307 (2006).
 - [19] C. Bunce, J. Wu, G. Ju, B. Lu, D. Hinzke, N. Kazantseva, U. Nowak, and R. W. Chantrell, *Phys. Rev. B* **81**, 174428 (2010).
 - [20] W. Hübner and K. H. Bennemann, *Phys. Rev. B* **53**, 3422 (1996).
 - [21] A. Fognini, G. Salvatella, R. Gort, T. Michlmayr, A. Vaterlaus, and Y. Acremann, *Struct. Dyn.* **2**, 024501 (2015).